Herschel: the first science highlights

LETTER TO THE EDITOR

The *Herschel* Lensing Survey (HLS): Overview[★,★★]

E. Egami[1], M. Rex[1], T. D. Rawle[1], P. G. Pérez-González[2,1], J. Richard[3], J.-P. Kneib[4], D. Schaerer[5,6], B. Altieri[7],
I. Valtchanov[7], A. W. Blain[8], D. Fadda[9], M. Zemcov[8,10], J. J. Bock[8,10], F. Boone[6,11], C. R. Bridge[8], B. Clement[4],
F. Combes[11], M. Dessauges-Zavadsky[5], C. D. Dowell[8,10], O. Ilbert[4], R. J. Ivison[12,13], M. Jauzac[4], D. Lutz[14],
L. Metcalfe[7], A. Omont[15], R. Pelló[6], M. J. Pereira[1], G. H. Rieke[1], G. Rodighiero[16], I. Smail[3], G. P. Smith[17],
G. Tramoy[4], G. L. Walth[1], P. van der Werf[18], and M. W. Werner[10]

(Affiliations are available in the online edition)

ABSTRACT

The *Herschel* Lensing Survey (HLS) will conduct deep PACS and SPIRE imaging of ~40 massive clusters of galaxies. The strong gravitational lensing power of these clusters will enable us to penetrate through the confusion noise, which sets the ultimate limit on our ability to probe the Universe with *Herschel*. Here we present an overview of our survey and a summary of the major results from our science demonstration phase (SDP) observations of the Bullet cluster ($z = 0.297$). The SDP data are rich and allow us to study not only the background high-redshift galaxies (e.g., strongly lensed and distorted galaxies at $z = 2.8$ and 3.2) but also the properties of cluster-member galaxies. Our preliminary analysis shows a great diversity of far-infrared/submillimeter spectral energy distributions (SEDs), indicating that we have much to learn with *Herschel* about the properties of galaxy SEDs. We have also detected the Sunyaev-Zel'dovich (SZ) effect increment with the SPIRE data. The success of this SDP program demonstrates the great potential of the *Herschel* Lensing Survey to produce exciting results in a variety of science areas.

Key words. infrared: galaxies – submillimeter: galaxies – galaxies: evolution – galaxies: high-redshift – galaxies: clusters: general

1. Introduction

With the successful launch and commissioning of the ESA's *Herschel* Space Observatory (Pilbratt et al. 2010), we are again on the verge of making great new discoveries. Following the breakthrough submillimeter/millimeter observations with SCUBA and MAMBO (cf., Blain et al. 2002), deep MIPS 24 μm observations carried out by the *Spitzer* Space Observatory have enabled us to trace the evolution of infrared-luminous galaxies up to $z \sim 3$–4 (e.g., Pérez-González et al. 2005; Le Floc'h et al. 2005). However, the validity of all these *Spitzer*-based results rests on the assumption that the total infrared luminosities of high-redshift infrared galaxies can be estimated accurately by sampling their rest-frame mid-infrared emission (e.g., the MIPS 24 μm band samples the rest-frame 8 μm emission at $z = 2$). Indeed, some *Spitzer* results have already questioned this assumption, suggesting that the use of local galaxy spectral energy distribution (SED) templates may lead to overestimating the total infrared luminosities of high-redshift galaxies (e.g., Papovich et al. 2007; Rigby et al. 2008). *Herschel* will allow us to measure the total infrared luminosities of a large number of high-redshift galaxies directly for the first time.

With *Herschel*, confusion noise produced by a sea of blended faint galaxies sets the ultimate limit on how deeply we can probe the Universe. Once the source confusion sets in, it is no longer possible to improve the detection limit by integrating longer. This limitation is especially severe for SPIRE, which reaches the confusion limit quickly.

To penetrate through the confusion limit, gravitational lensing by massive galaxy clusters offers a very powerful and yet cheap solution (e.g., Blain 1997). Magnification factors of 2–4× are quite common in the cluster core regions, and when a background source is strongly lensed (i.e., multiply imaged), magnification factors can reach 10×–30× or more. Note that a magnification factor of 10× corresponds to a factor of 100× saving in observing time when the sensitivity is background-limited. Therefore, a fairly short-integration image of a cluster core region would often reveal sources that are well below the detection limit of an ultra-deep blank-field image. This method was for example employed for the first SCUBA observations of the high-redshift Universe, which resulted in the identification of the substantial population of infrared-luminous galaxies at $z > 1$ (Smail et al. 1997).

The use of gravitational lensing is especially powerful at infrared/submillimeter wavelengths. This is because cluster cores are dominated by early-type galaxies, which usually emit little at these wavelengths. Therefore infrared/submillimeter sources detected in cluster cores are often background galaxies. In other words, when observed at these wavelengths, massive cluster cores virtually act as a transparent lens. Lensing studies in the infrared/submillimeter also benefit from the steep galaxy counts at these wavelengths.

These types of lensing surveys, however, have one limitation: the small number of strongly lensed galaxies observed per cluster. Although a large number of massive clusters have been targeted by ground-based submillimeter/millimeter observations (e.g., Smail et al. 2002; Chapman et al. 2002; Knudsen et al. 2008), the number of strongly lensed (i.e., multiply imaged) galaxies discovered in these surveys remains small: for example, the $z = 2.5$ galaxy in Abell 2218 (Kneib et al. 2004), the $z = 2.9$ galaxy in MS0451.6-0305 (Borys et al. 2004), the $z = 2.8$ galaxy in the Bullet cluster (Wilson et al. 2008; Gonzalez et al. 2009; Rex et al. 2009; Johansson et al. 2010), and most recently the exceptionally bright $z = 2.32$ galaxy in MACSJ2135-0102 (Swinbank et al. 2010). Based on these observations, we empirically estimate the rate of finding these strongly lensed infrared/submillimeter galaxies to be roughly 1 in 10 with the sensitivity of ground submillimeter observations (e.g., SCUBA, LABOCA). Therefore many tens of clusters need to be observed to study a significant number of strongly lensed galaxies.

2. The *Herschel* Lensing Survey (HLS)

As a *Herschel* open-time key program, we are conducting exactly such a large lensing survey, targeting ∼40 massive clusters of galaxies ("The *Herschel* Lensing Survey (HLS)", PI – Egami, 292.3 h). Together with the PACS and SPIRE Guaranteed-Time teams, which will observe 10 clusters (Altieri et al. 2010; Blain et al., in prep.), we will obtain deep images with PACS (Poglitsch et al. 2010) at 100 and 160 μm and SPIRE (Griffin et al. 2010) at 250, 350, and 500 μm for a sample of ∼50 massive clusters as a legacy of the *Herschel* mission.

Target selection – As the targets of the survey, we chose the most X-ray-luminous clusters from the ROSAT X-ray all-sky survey assuming that the most X-ray-luminous clusters are also the most massive and therefore the most effective gravitational lenses. The majority of our targets come from the sample of the Local Cluster Substructure Survey (LoCuSS) (e.g., Smith et al. 2010), which adopts the following selection criteria: (1) $L_X > 2 \times 10^{44}$ erg/s, (2) $0.15 < z < 0.3$, (3) $N_{HI} < 7 \times 10^{20}$ cm^{-2}, and (4) $-70 < \delta < 70$. In addition, some number of clusters with spectacular lensed systems were included in the sample. For the majority of our target clusters, we have well-constrained accurate mass models, which have been constructed through many years of intensive imaging/spectroscopic campaigns with HST, Keck, and VLT telescopes. Other important considerations were the availability of MIPS 24 μm images and accessibility from ALMA for future follow-up observations although these conditions were not always met.

Observing parameters – Each target cluster is imaged by both PACS (100 and 160 μm) and SPIRE (250, 350, and 500 μm). With PACS we use the scan-map mode with the medium speed (some early data were taken with the slow speed). The scan leg lengths are 4′, cross-scan step is 20″, number of scan legs is 13. Each cluster is observed twice by orthogonal scan maps (map orientation angles of 45° and 315°) with 18 repetitions each. The total observing time is 4.4 h per cluster with an on-source integration time of 1.6 h (1500 s/pixel).

With SPIRE we use the Large Map mode with the nominal speed. The scan direction was set to scan angles A and B. The length and height of the map are set to 4′, which in practice will produce a map of 17′×17′. With 20 repetitions, the total observing time per cluster is 1.7 h with an on-source integration time of 0.6 h (17 s/pixel).

Coordinated programs – The *Herschel* Lensing Survey is directly coordinated with a few other observing programs.

The most important is the *Spitzer*/IRAC Lensing Survey (PID 60034; "The IRAC Lensing Survey: Achieving JWST Depth with Spitzer", PI – Egami, 526 h), which is one of the *Spitzer* Warm-Mission Exploration Science programs. This program will obtain deep (5 h/band) *Spitzer*/IRAC 3.6 and 4.5 μm images of ∼50 massive clusters. By design, its target list is highly overlapped with that of the HLS. Deep IRAC images will be essential for identifying optically-faint high-redshift infrared-luminous galaxies as well as for deriving accurate photometric redshifts. In addition, roughly half of the HLS clusters are imaged by HST/WFC3 through two on-going programs (GO 11592: "Are Low-Luminosity Galaxeis Responsible for Reionization?", PI – Kneib, 43 orbits; MCT: "Through a Lens, Darkly – New Constraints on the Fundamental Components of the Cosmos", PI – Postman, 524 orbits).

The *Herschel* Lensing Survey is also closely related to two other *Herschel* open-time key programs: "LoCuSS: A Legacy Survey of Galaxy Clusters at $z = 0.2$" (Smith et al. 2010) and "Constraining the Cold Gas and Dust in Cluster Cooling Flows" (Edge et al. 2010a,b). The former will obtain wide (30′ × 30′) and shallow PACS 100/160 μm maps of ∼30 massive galaxy clusters at $z \sim 0.2$, many of which are also targeted by the HLS. Note that the HLS SPIRE maps cover a significant part (the central 17′×17′) of the LoCuSS PACS maps, leading to a natural collaboration between the two teams. The latter program will study the brightest cluster galaxies (BCGs) in a dozen cooling-flow clusters, and the HLS data will provide PACS/SPIRE photometry for a much larger sample of BCGs.

3. Science demonstration target: the Bullet cluster

In the science demonstration phase (SDP), we observed the Bullet cluster at $z = 0.297$ (1E0657-56=RXCJ 0658.5-5556). The Bullet cluster was targeted because (1) there is a strongly lensed bright submillimeter/millimeter galaxy at $z = 2.8$ (see the Introduction); (2) it has a large amount of ancillary data (see Appendix A); and (3) it is in the continuous viewing zone of *Herschel*.

3.1. Data processing

Raw *Herschel* data products were reduced with the common pipeline procedures distributed within the *Herschel* interactive processing environment (HIPE) (Ott 2010). Deviations from the standard routines are described below.

PACS — The PACS observations were affected by erroneous flashes of the calibration lamp at the end of each scan repetition. These high-intensity spikes in the detector time-streams were followed by an exponential decay in the signal while the bolometers re-thermalized. While the spike and a large fraction of the decay occurred during the slew between repetitions, the bolometers were not fully stabilized until after the beginning of the next scan, resulting in a ∼10 % reduction of usable data.

The *1/f* noise drift in the PACS bolometers was removed by a high-pass filter. Before applying the filter, bright sources (>5σ) were masked to prevent Fourier ringing about their positions. These sources were selected from an unmasked first-pass of the 160 μm map, and the allocated mask size was proportional to their significance. High-pass filter lengths of 30 and 40 time-stream frames were used for PACS 100/160 μm data respectively. These lengths were selected to minimize residual *1/f* noise in the resultant maps without clipping power on the scale of the PSF. The maps incorporate all data observed, while the telescope maintained the nominal scan speed (including some turnaround data). The final PACS maps have pixel sizes of 2″ and 3″ (100/160 μm).
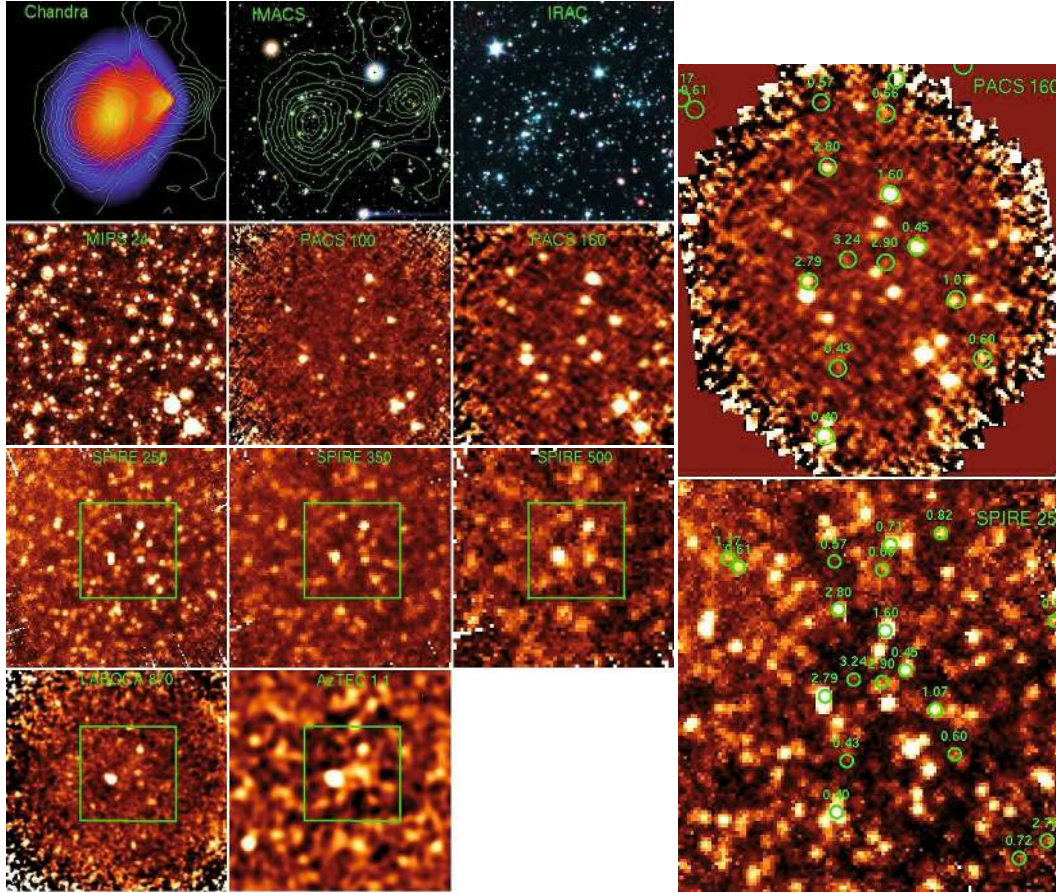
Fig. 1. *Left* – Multi-wavelength imaging data of the Bullet cluster as indicated in each panel (see Appendix A for references). The contours overlaid on the Chandra and IMACS images are the weak-lensing mass map from Clowe et al. (2006). The field of view is ∼7′×7′ in the top two rows and ∼15′×15′ in the bottom two rows (the ∼7′×7′ area is indicated with the squares); *Right* – Spectroscopic and photometric redshifts overlaid on the PACS 160 μm map (*top*) and SPIRE 250 μm map (*bottom*). See Rex et al. (2010) for the full source list.

Table 1. The HLS Bullet cluster data.

Instrument	FOV (arcmin)	λ (μm)	beam (arcsec)	Depth (5σ, mJy)
PACS	∼8 × 8	100	7.7	5.5 ± 0.7
		160	12.0	10 ± 1
SPIRE	∼17 × 17	250	18	12 ± 2
		350	25	17 ± 3
		500	36	18 ± 4

SPIRE — In addition to the nominal scan legs (speed = 30″ s^{-1}) we included all turnaround data observed while the telescope was scanning faster than 0′.5 s^{-1}, which greatly increased the coverage of the outer regions. Low-frequency drifts in the SPIRE detectors were removed by subtracting the median value of the nominal scan-speed data from each individual scan leg independently. The final SPIRE maps have pixel sizes of 6″, 9″, and 12″ (250/350/500 μm respectively).

The properties of the processed PACS and SPIRE maps are summarized in Table 1.

3.2. Overview of the Bullet cluster SDP data

Figure 1 shows the PACS and SPIRE images of the Bullet cluster. Also shown are the Chandra, Magellan/IMACS, *Spitzer*/IRAC & MIPS 24 μm, LABOCA and AzTEC images of the same field (see Appendix A for references). As expected, the MIPS 24 μm observation goes deep enough to detect the counterparts for most of the PACS/SPIRE sources. This means that one immediate goal of *Herschel* will be to determine

the far-infrared SEDs of 24 μm-detected sources. Indeed, the MIPS 24 μm image enables us to accurately extract fluxes from confused *Herschel* sources (Pérez-González et al. 2010). However, the most interesting type of *Herschel* sources may be those without 24 μm counterparts (such a source has not yet been identified in our data).

We detected two significantly lensed galaxies in the Bullet cluster field, one at $z = 2.79$ and the other at $z = 3.24$ (Rex et al. 2010; Pérez-González et al. 2010). With magnification factors of >54 and 11.3 (Paraficz et al., in prep.) their intrinsic total infrared luminosities are <5×10^{11} $L_\odot$ and 3.5×10^{11} $L_\odot$. Figure 1 shows the locations of these two and other background galaxies studied. Note that only HLS can detect luminous infrared galaxies (LIRGs; $10^{11} < L_{\rm TIR} < 10^{12}$ $L_\odot$) at $z > 2$–3 in both PACS and SPIRE data.

One major finding of this SDP program is the diversity of far-infrared/submillimeter SEDs seen with the $z = 0.3$ cluster-member galaxies, $z = 0.35$ background group galaxies, and higher-redshift field galaxies behind these two galaxy concentrations (Rawle et al. 2010; Rex et al. 2010). This is shown in Fig. 2, which compares the total infrared luminosities measured by fitting the Rieke et al. (2009) SED templates to the observed data points (Measured $L_{\rm TIR}$) against the total infrared luminosity classes originally assigned to these SED templates (Template $L_{\rm TIR}$). Although these two luminosities agree for many of the cluster and background group members, Template $L_{\rm TIR}$ is significantly lower than Measured $L_{\rm TIR}$ for most of the higher-redshift background galaxies. What this means is that the shapes of the
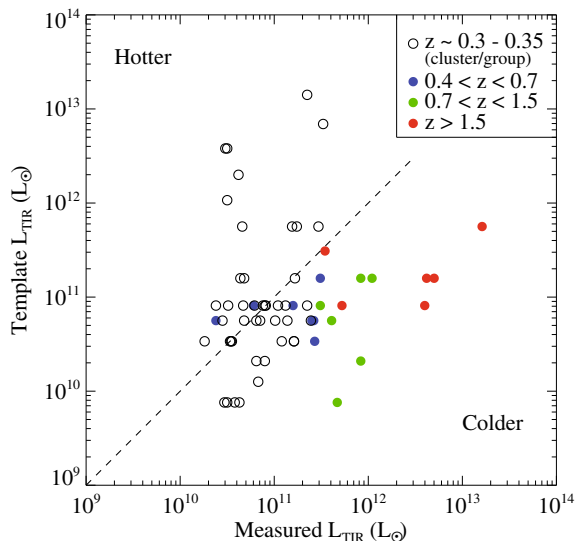
Fig. 2. Comparison between the total infrared luminosities measured by fitting the Rieke et al. (2009) SED templates to the observed data points (Measured L_{TIR}) and the total infrared luminosity classes originally assigned to these SED templates (Template L_{TIR}). The open circles denote the members of the Bullet cluster and background group, while the solid circles denote the galaxies behind these two systems. Galaxies below the 1:1 correspondence (dashed line) have SEDs that resemble lower-luminosity local SED templates (i.e., with colder dust temperatures). Galaxies above the line have the opposite characteristics. The distribution of the points along the Y axis is discreet because of the finite number of templates available in the model. See Rex et al. (2010) and Rawle et al. (2010) for more detail.

infrared/submillimeter SEDs of these galaxies resemble those of lower-luminosity galaxies in the local Universe. This result is consistent with the earlier findings by various *Spitzer* observations (e.g., Papovich et al. 2007; Rigby et al. 2008). This also implies that these higher-redshift star-forming galaxies have a larger amount of colder dust compared to the local galaxies with similar infrared luminosities.

In the face of this SED difference, the recent finding is surprising that the total infrared luminosities can be estimated fairly well (at least up to $z \sim 1.5$) if we use the luminosity-dependent galaxy SED templates as observed locally (Elbaz et al. 2010). We confirmed this finding with our Bullet cluster data. Despite this agreement, however, we also found that the kind of SED mismatch seen in Fig. 2 clearly exists in the data even at $z < 1$ (Rex et al. 2010). This suggests that the good match between the observed and 24 μm-derived total infrared luminosities does not necessarily mean that the local SED templates provide good fits to the observed SEDs. A more detailed study of a larger sample is required to resolve this issue.

Equally interesting is the discovery of cluster/group-member galaxies that show large deviations in the opposite direction (Rawle et al. 2010). In other words, the SEDs of these galaxies resemble those of higher-luminosity galaxies in the local Universe. These galaxies therefore are likely to have a larger amount of hotter dust and a more pronounced infrared SED peak compared to the local counterparts with similar infrared luminosities. Similar galaxies were also found in other clusters (Pereira et al. 2010; Smith et al. 2010), which possibly suggests that this type of SEDs may be specific to the cluster environment.

Finally, we also report the first detection of the Sunyaev-Zel'dovich (SZ) effect increment at 350 and 500 μm using the SPIRE data (Zemcov et al. 2010). The measurements will allow us to assess the relativistic correction to the SZ effect.

4. Conclusions

The SDP observations of the Bullet cluster clearly demonstrate the great potential of the HLS in a variety of science areas. With the *Herschel* observations nearly done, HLS is expected to make a rapid progress in the near future. One immediate interest is whether it can find strongly lensed sources that are bright enough to perform spectroscopy with *Herschel*. Ultimately we will construct a definitive sample of ~50 lensing clusters with a variety of multi-wavelength data and accurate mass models. This data set can be further exploited by future facilities such as ALMA, JWST, SPICA, and ground 30-m class telescopes.

References

Altieri, B., et al. 2010, A&A, 518, L17
Blain, A. W. 1997, MNRAS, 290, 553
Blain, A. W., Smail, I., Ivison, R. J., Kneib, J., & Frayer, D. T. 2002, Phys. Rep., 369, 111
Borys, C., Chapman, S., Donahue, M., et al. 2004, MNRAS, 352, 759
Chapman, S. C., Scott, D., Borys, C., & Fahlman, G. G. 2002, MNRAS, 330, 92
Clowe, D., Bradač, M., Gonzalez, A. H., et al. 2006, ApJ, 648, L109
Edge, A. C., et al. 2010a, A&A, 518, L46
Edge, A. C., et al. 2010b, A&A, 518, L47
Elbaz, D., et al. 2010, A&A, 518, L29
Gonzalez, A. H., Clowe, D., Bradač, M., et al. 2009, ApJ, 691, 525
Griffin, M. J., et al. 2010, A&A, 518, L3
Johansson, D., Horellou, C., Sommer, M. W., et al. 2010, A&A, 514, A77
Kneib, J., van der Werf, P. P., Kraiberg Knudsen, K., et al. 2004, MNRAS, 349, 1211
Knudsen, K. K., van der Werf, P. P., & Kneib, J. 2008, MNRAS, 384, 1611
Le Floc'h, E., Papovich, C., Dole, H., et al. 2005, ApJ, 632, 169
Ott, S. 2010, in Astronomical Data Analysis Software and Systems XIX, ed. Y. Mizumoto, K.-I. Morita, & M. Ohishi, ASP Conf. Ser., in press
Papovich, C., Rudnick, G., Le Floc'h, E., et al. 2007, ApJ, 668, 45
Pereira, M., et al. 2010, A&A, 518, L40
Pérez-González, P. G., Rieke, G. H., Egami, E., et al. 2005, ApJ, 630, 82
Pérez-González, P. G., et al. 2010, A&A, 518, L15
Pilbratt, G. L., et al. 2010, A&A, 518, L1
Poglitsch, A., et al. 2010, A&A, 518, L2
Rawle, T. D., et al. 2010, A&A, 518, L14
Rex, M., Ade, P. A. R., Aretxaga, I., et al. 2009, ApJ, 703, 348
Rex, M., et al. 2010, A&A, 518, L13
Rieke, G. H., Alonso-Herrero, A., Weiner, B. J., et al. 2009, ApJ, 692, 556
Rigby, J. R., Marcillac, D., Egami, E., et al. 2008, ApJ, 675, 262
Smail, I., Ivison, R. J., & Blain, A. W. 1997, ApJ, 490, L5
Smail, I., Ivison, R. J., Blain, A. W., & Kneib, J. 2002, MNRAS, 331, 495
Smith, G. P., et al. 2010, A&A, 518, L18
Swinbank, A. M., Smail, I., Longmore, S., et al. 2010, Nature, 464, 733
Wilson, G. W., Hughes, D. H., Aretxaga, I., et al. 2008, MNRAS, 390, 1061
Zemcov, M., et al. 2010, A&A, 518, L16

Appendix A: Ancillary data for the Bullet cluster

Table A.1. The Bullet cluster ancillary data.

Facilities	Bands	Ref.
	Imaging	
Magellan/IMACS	*B*, *V*, *R*	1
HST/ACS	*F*606*W*, *F*775*W*, *F*850*LP*	2
VLT/HAWK-I	*Y*, *J*	3
Spitzer/IRAC	3.6, 4.5, 5.8, & 8.0 μm	2
Spitzer/MIPS	24 μm	2
LABLOCA	870 μm	4
AzTEC	1.1 mm	5
	Spectroscopy	
Magellan/IMACS	optical (856 targets)	6
Blanco/Hydra	optical (202 targets)	7
VLT FORS	optical (14 targets)	8

References. (1) Clowe et al. (2006); (2) Gonzalez et al. (2009); (3) J.-G. Cuby, priv. comm.; (4) Johansson et al. (2010); (5) Wilson et al. (2008); (6) Chung et al. (2010) (7) D. Fadda, priv. comm.; (8) J. Richard, priv. comm.

[1] Steward Observatory, University of Arizona, 933 N. Cherry Ave, Tucson, AZ 85721, USA
e-mail: eegami@as.arizona.edu

[2] Departamento de Astrofísica, Facultad de CC. Físicas, Universidad Complutense de Madrid, 28040 Madrid, Spain

[3] Institute for Computational Cosmology, Department of Physics, Durham University, South Road, Durham DH1 3LE, UK

[4] Laboratoire d'Astrophysique de Marseille, CNRS - Université Aix-Marseille, 38 rue Frédéric Joliot-Curie, 13388 Marseille Cedex 13, France

[5] Geneva Observatory, University of Geneva, 51, Ch. des Maillettes, 1290 Versoix, Switzerland

[6] Laboratoire d'Astrophysique de Toulouse-Tarbes, Université de Toulouse, CNRS, 14 Av. Edouard Belin, 31400 Toulouse, France

[7] *Herschel* Science Centre, ESAC, ESA, PO Box 78, Villanueva de la Cañada, 28691 Madrid, Spain

[8] California Institute of Technology, Pasadena, CA 91125, USA

[9] NASA *Herschel* Science Center, California Institute of Technology, MS 100-22, Pasadena, CA 91125, USA

[10] Jet Propulsion Laboratory, Pasadena, CA 91109, USA

[11] Observatoire de Paris, LERMA, 61 Av. de l'Observatoire, 75014 Paris, France

[12] UK Astronomy Technology Centre, Science and Technology Facilities Council, Royal Observatory, Blackford Hill, Edinburgh EH9 3HJ, UK

[13] Institute for Astronomy, University of Edinburgh, Blackford Hill, Edinburgh EH9 3HJ, UK

[14] Max-Planck-Institut für extraterrestrische Physik, Postfach 1312, 85741 Garching, Germany

[15] Institut d'Astrophysique de Paris, CNRS and Université Pierre et Marie Curie, 98bis Boulevard Arago, 75014 Paris, France

[16] Department of Astronomy, University of Padova, Vicolo dell'Osservatorio 3, 35122 Padova, Italy

[17] School of Physics and Astronomy, University of Birmingham, Edgbaston, Birmingham, B15 2TT, UK

[18] Sterrewacht Leiden, Leiden University, PO Box 9513, 2300 RA Leiden, the Netherlands